IEEE Access
Multidisciplinary | Rapid Review | Open Access Journal

Received July 20, 2021, accepted July 23, 2021, date of publication August 6, 2021, date of current version August 16, 2021.

Digital Object Identifier 10.1109/ACCESS.2021.3102942

Microwave Polarizer Based on Complementary Split Ring Resonators Frequency-Selective Surface for Conformal Application

WEI LI[1], YU LAN[2,3], HUANPENG WANG[2], AND YUEHANG XU[2,3], (Senior Member, IEEE)

[1]CETC Information Science Academy, Beijing 100086, China
[2]Key Laboratory of Integrated Circuits and Systems in Nantaihu New Area, Yangtze Delta Region Institute (Huzhou), University of Electronic Science and Technology of China, Huzhou 313001, China
[3]School of Electronic Science and Engineering, University of Electronic Science and Technology of China, Chengdu 611731, China

Corresponding author: Yuehang Xu (yuehangxu@uestc.edu.cn)

This work was supported by the National Key Research and Development Project under Grant 2019YFB1706802.

ABSTRACT In this paper, a microwave polarizer based on frequency selective surface (FSS) loaded with complementary split ring resonator (CSRR) for non-planar and conformal application is presented. The frequency-selective polarizer is fabricated on liquid crystal polymer substrates (LCPs) material with 50μm thickness, which shows very good mechanical flexibility for microwave band. The Frequency-selective polarizer consists of a metal FSS screen pair with double complementary split ring resonators aligned in the vertical direction without any displacement. The substrate integrated waveguide (SIW) cavity was introduced to enhance the Q-factor of the CSRR particles and the mechanical strength of the FSS screens at bending conditions. The measured results show that the CSSR-FSS polarizer with the minimum transmission loss for TE-polarization incidence wave is 0.75dB at the 10.24 GHz and 19.05 dB for TM-polarization incidence wave, with an extinction ratio of 18.3dB. Finally, the oblique incidence from normal to 60 degrees and bending tests with the bending radius of 9.8 cm and 8.8 cm of the CSRR-FSSs were also carried out, and the measured results indicate that the CSRR-FSS show a low susceptibility to bending behavior at the small bending radius beyond the 8.8 cm and different incidence angles from normal to 45 degrees. Both the simulated and experiment data indicated that the proposed ultra-thin CSRR-FSS shows excellent flexibility and polarization selectivity.

INDEX TERMS Frequency selective surface, complementary split ring resonators, liquid crystal polymer substrate, bending effect, polarizer.

I. INTRODUCTION

In recently years, controlling the polarization state of the electromagnetic wave has been becoming an intense research field for many applications from microwave to optical regimes [1]. In traditional way, the polarization beam splitters are used for getting one single polarization [2], [3]. While adding another component, which inevitably increased the complexities of the existing systems. To solve the above-mentioned contradiction and miniaturizing the whole systems, the polarizer is used to transit the wanted polarization wave and extinguish the unwanted polarization wave by reflection, redirection or absorption [4], such as many polarizers [5]–[7] which are working at the light regime. Although the aforementioned polarizers show good performance of high extinction ratio, it is difficult to extend to the microwave frequency.

Frequency selective surface (FSS) loaded on periodic functional elements are usually used as space filters, polarizers and subreflectors are used in stealthy aircraft antennas for reducing the radar cross section (RCS) [8], [9] in microwave and millimeter wave's applications. The split ring resonator (SRR), as shown Fig.1(a), was usually proposed for designing of artificial magnetic [10] which always applied to negative magnetic permeability media [11] and left-hand metamaterials [12]. Recently, some FSSs load on the SRR elements for polarization-relative applications are reported, such as a 10GHz band-pass isotropic FSS made of cubic arrangements of SRRs elements [13] and a circular polarizer consisting of a twisted double SRRs [14], etc. However, a problem emerges as the SRR-FSSs was developed: these SRR-FSSs always show a stop-band behavior at the frequency of resonance of

The associate editor coordinating the review of this manuscript and approving it for publication was Wen-Sheng Zhao.

This work is licensed under a Creative Commons Attribution 4.0 License. For more information, see https://creativecommons.org/licenses/by/4.0/

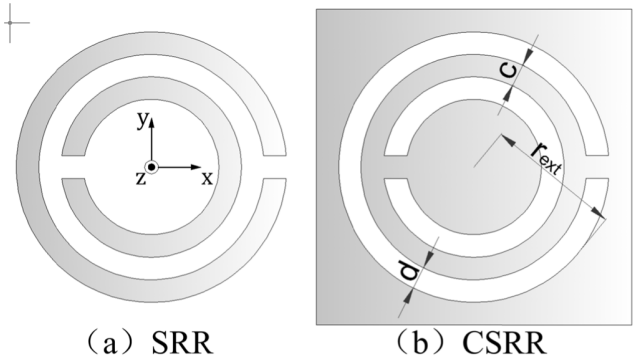

FIGURE 1. Geometries of the SRR(a) and the CSRR(b) particles (gradation gray area is the metal strips).

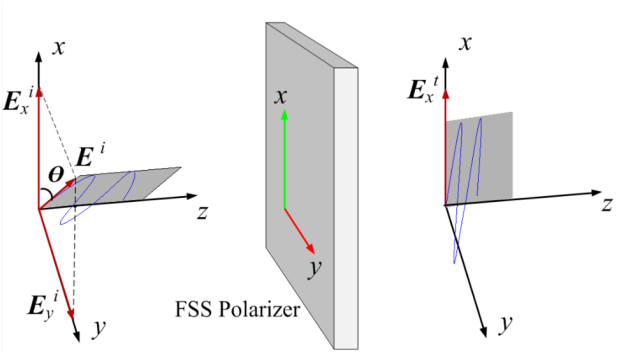

FIGURE 2. Schematic topology of frequency selective polarizer. In this configuration, the incidence electric field vector is titled θ degrees relative to x-z plane. After passing through the FSS polarizer, the transmission electric field vector only left the x component.

the SRRs, which coincided with the band-stop FSSs loaded on metal patch elements [15]. Based on the Babinet principle [16], the complementary split ring resonator (CSRR) shown in Fig.1(b) could be loaded on the FSS surface, forming the CSRR-FSSs with pass-band behavior at the resonance frequency of the CSRRs particle [17], [18]. This kind of SRRs/CSRRs units take the advantages of small electrical size at resonance, strong magnetic moment and electrical dipole simultaneously when the SRRs resonance are excited by an appropriate polarization incidence [19], [20].

The Ref. [17]–[20] had made some theory analysis for the SRR/CSRR particles and predicted that SRR/CSRR-FSSs permit resonance to occur at the frequency of resonance of the SRR/CSRRs for appropriate polarization plane wave excitation. However, the orthogonal polarization excitation is non-resonant, implying the SRR/CSRR-FSSs would be considered as polarizers at the near resonance frequency of the SRR/CSRR particles. There is no experimental result shows the combination of the frequency-selective and polarization-selective properties based on CSRRs particles for the designing of FSS polarizers at microwave and millimeter applications yet.

In the last decade, with the development of the wearable and portable electric devices, the flexible materials and non-planar and conformal applications were widely concerned in RF/microwave/millimeter-wave and biomedical applications, such as: wearable devices mounted on the skins collecting the health information from bodies [21] and a metamaterial-skin consist of an array of liquid metallic split ring resonance (SRRs) embedded in a flexible elastomer for the cloaking applications [22]. In this article, the liquid crystal polymer (LCP) substrate was chosen to design the microwave FSS polarizer and the aligned complementary split ring resonators pair was printed on both sides of an ultrathin dielectric LCP substrate Rogers 3850 [23], applying for flexible and non-planar surroundings [24]–[26] in the future.

The outline of this paper is organized as follows: Section II presents design processes and the fabrication prototype of the proposed CSRR-FSS polarizer. In section III, the experimental results of the CSRR-FSS polarizer at oblique incidence and bending conditions are presented and analyzed. Finally, the conclusion for this work is demonstrated in section IV.

II. DESIGN AND RESULT

Fig.2 gives the primary function concept of the FSS polarizer proposed in this paper. The operation principle of the FSS screen polarizer is that it has the ability to significantly suppress the transmission of one direction polarization incidence wave, while well guiding the orthogonal polarization incidence wave with little or no attenuation.

In this case, for the convenience of the analysis, we defined the x axis is the transmission direction, and the y axis is the suppressing direction. The function of the $F(\theta)$ is introduced to describe the distinct properties of the FSS polarizer for vertical and horizontal components incidence as followed:

$$F(\theta) = \begin{cases} 1, & \theta = 0°, 180° \\ 0, & \theta = \pm 90° \end{cases} \tag{1}$$

The FSS screen is illuminated by the incidence wave with the electric field vector E^i titled θ degrees relative to x-z plane and the E_x^i and E_y^i are the vertical and horizontal electric field components of the incidence wave, respectively. Because the FSS screen behaviors have different properties for the vertical (E_x^i) and horizontal components (E_y^i) of the incidence wave and any kind of electric field vectors of the incidence wave could be expressed using the two orthogonal components. So, we can express the transmission wave (E_x^t, E_y^t) using the terms of the incidence wave (E_x^i, E_y^i) as the following formulas:

$$\begin{pmatrix} E_x^t \\ E_y^t \end{pmatrix} = A \times \begin{pmatrix} F(\theta)_{\theta=0°,180°} & F(\theta)_{\theta=90°} \\ F(\theta)_{\theta=90°} & F(\theta)_{\theta=0°,180°} \end{pmatrix} \tag{2}$$

with

$$A = \begin{pmatrix} T_x E_x^i & T_{xy} E_y^i \\ T_y E_y^i & T_{yx} E_x^i \end{pmatrix} \tag{3}$$

If we consider the crossed transmission coefficients is to be negligible [27] (i.e. $T_{xy} = 0$ and $T_{yx} = 0$). From the formulas from the (1) - (3), we can get that:

$$\begin{pmatrix} E_x^t \\ E_y^t \end{pmatrix} = \begin{pmatrix} T_x E_x^i \\ 0 \end{pmatrix} \tag{4}$$

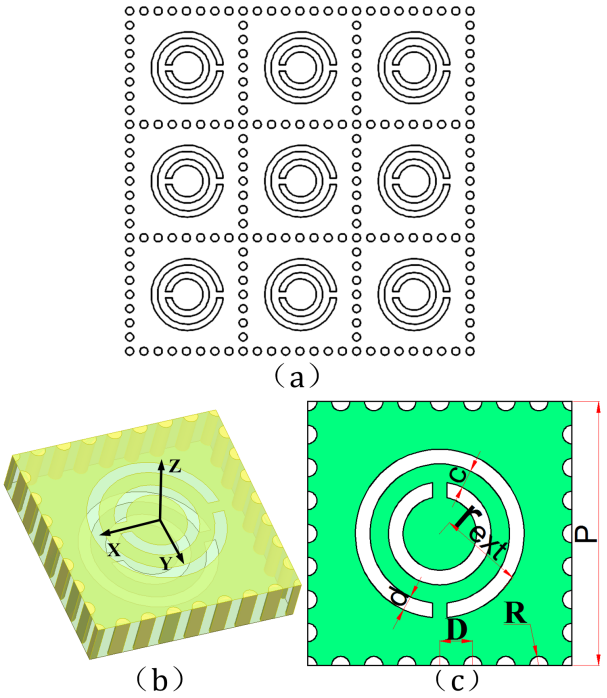

FIGURE 3. (a) The function array of the polarizer (b) The unit element of the polarizer, (c) Parameters of the unit element: P=7.2mm, D=0.9mm, R=0.25mm, d=0.4mm, c=0.5mm, r_{ext}=2.3mm.

From the formulas (4), the transmission waves only leave the x axis components and filter the orthogonal direction y components, which coincide with the FSS polarizer transmission direction.

The proposed frequency-selective polarizer, as shown in Fig.3(a), is fabricated using the cells Fig.3(b) which comprised by two metal layers loaded with CSRRs particles and one clamped dielectric layer 3850. For the frequency-selective polarizer cells, a double CSRRs pair is aligned along the z axis with no displacement and surrounded by periodic metal cylinders, forming the substrate integrated waveguide (SIW) cavity.

The metallic layers lie in x-y plane with a thickness of $t = 18\mu$m and the dielectric layers 50 μm LCP substrate with constant relative permittivity ε_r=3.0 and loss tangent of 0.0025. The CSRR unit is processed by etching two open-loop rings through the metallic plane, and the radius and size of the gaps of the CSRRs control the operation frequencies of the frequency-selective polarizer. Fig.3(c) gives the parameters of the CSRR unit for the design of the frequency-selective polarizer proposed in this paper.

A. CHARACTERISTICS OF THE SUBSTRATE INTEGRATED WAVEGUIDE CAVITY RESONANCES

The substrate integrated waveguide technique has been used to keeps the advantages of conventional metallic waveguide's properties of high Q-factor, high selectivity and high-power capacity etc. at the planar integrated circuits applications [28]–[30]. Another advantage is that the SIW cavity increase the mechanical strength of the FSS screen for small bending application.

In general, the SIW structure resonance could only support TM_{mn0} ($m = 1, 2, 3\ldots$. and $n = 1, 2, 3\ldots$.) modes, considering the coordinate definitions used as Fig. 1(a). The TE mode resonance could not exist in the SIW box, because that the electric current at the z- direction only can flow the via holes, which current distribution could not support the TE mode field distributions. And its resonance frequency of f_{SIW} of TE_{mn0} modes could be determined by formula (5) (for square element):

$$f_{SIW,TM_{mno}} = \frac{c_0}{2\sqrt{\varepsilon_r}}\sqrt{\left(\frac{m}{P_{eff}}\right)^2 + \left(\frac{n}{P_{eff}}\right)^2} \tag{5}$$

with

$$P_{eff} = P - \frac{(2R)^2}{0.95D} \tag{6}$$

where the R stand for the radius of the via holes, D for the space between the two holes, P stand for the width or length for the SIW resonance cavity, and the c_0 and ε_r is the light speed in vacuum and the relative dielectric permittivity of the substrates, respectively. The dimensions of P_{eff} parameter is the effect length relating the SIW cavity to a metallic rectangular cavity, and the m and n are the mode numbers for the SIW resonance cavity. We choose the periodical lattice of the CSRR element as $P = 7.2$mm, which lead the f_{SIW} resonance frequency of TE_{120} mode (about 27GHz) made by the SIW cavity far away from the CSRR-FSS desire operation frequency (about 10GHz) [31], avoiding the increasing dispensable variables influences for the analyzing of the CSRR-FSS polarizer screens and the higher possibility of appearance of grating lobes around the passband because of the too large size of the periodic SIW cavity [32], [33], respectively.

B. CHARACTERISTICS OF BASIC CSRR-FSS FREQUENCY RESPONSE

Figure.3 gives the geometries of the SRR/CSRR particle, and the particles would resonate at the angular frequency ω_0:

$$\omega_0 = \sqrt{\frac{2}{\pi r_0 C_0 L}} \tag{7}$$

where L is the inductance of an average ring radius $r_0 = r_{ext}$-c-$d/2$ which c is the width gap. And C_0 is the equivalent capacitance of unit length between the outer and inner rings.

Fig. 4 shows the comparison of frequency response for TE-polarization and TM-polarization incidence waves among the single/double metal screen CSRR-FSS and a single/double metal screen CSRR-FSS loaded with LCP substrate with the same CSRRs elements and periodicity. As we can see, for the TE-polarization incidence wave, the loading dielectric between the metallic screen would make the resonance frequency of the FSS shift to lower end, and the bandwidth of the double cascading FSS screens would be wider than single FSS screens which is caused by the coupling between the two metallic screens. The transmission

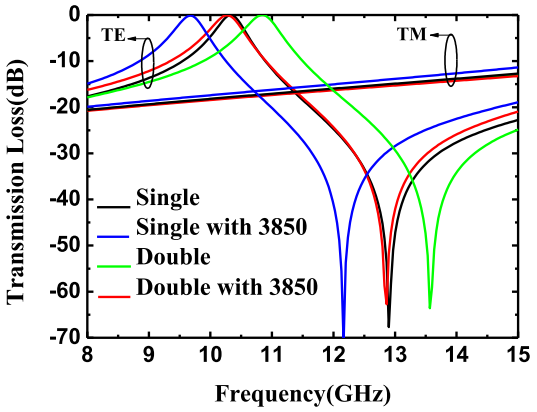

FIGURE 4. Frequency response of ideal single/double screen FSS polarizer and single/double screen FSS polarizer loaded on LCP dielectric 3850 with the same dimensions and periodicity, for TE-polarization and TM-polarization incidence wave.

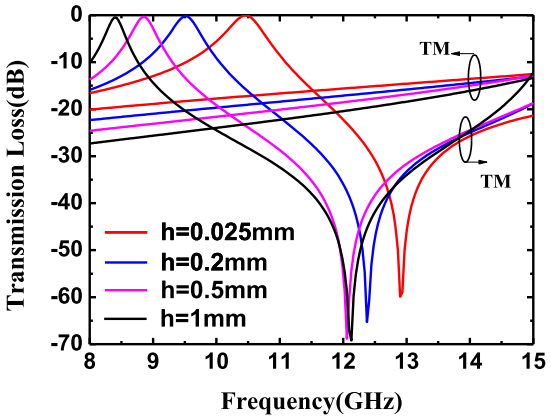

FIGURE 5. Frequency response of double cascading SCRR-FSS screens loaded on LCP dielectric with different thickness of dielectric slab for TE-polarization and TM-polarization incidence wave.

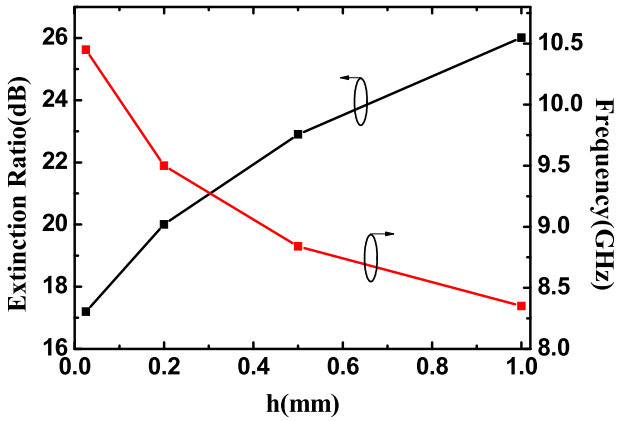

FIGURE 6. The operation Frequency and extinction ratio (ER) of double cascading SCRR-FSS polarizer screens loaded on LCP dielectric with different thickness of dielectric slab from 0.025mm to 1mm.

nulls of the CSRR-FSSs beyond the higher pass-band are caused by the inter-coupling effect between the etched two open-loop rings in the same CSRR elements. A relatively sharp stop-band suppression is formed by the transmission null. For the TM polarization incidence wave, the characteristics of the transmission loss almost have no influence.

C. INFLUENCE OF THICKNESS OF LOADED DIELECTRIC

The thickness of the dielectric is an important parameter for the cascading FSS screens. In general, for the conventional slot array FSSs screens, increasing the thickness of the dielectric slab would make the resonance frequency of the slot periodic decreased and the bandwidth increased. When the thickness of the substrate slab increased to greater than half wavelength of the resonance frequency of the FSS screen, the side lobes would be closer to the passband and the performance deterioration of the transmission loss in passband is always unacceptable anymore, so the thickness of the substrate slabs is better to be set less than half wavelength of the FSSs operation frequency [28].

Fig.5 shows performance changes of the double cascading CSRR-FSS screen loaded with substrate which is proposed in this paper, with different dielectric thickness(h) from 0.025 mm to 1 mm. The dimensions and periodicity of the CSRR elements are presented in Fig.2, but without the substrate integrated waveguide structures. From the Fig.5 we can find that, with the increasing of the thickness of the dielectric slabs, the operation frequency of the CSRR-FSS polarizers would be shifted to the lower end from 10.5GHz at 0.025mm to 8.4GHz at 1mm and the extinction ratio(ER) which defined as the ratio of the TE-polarization transmission power to TM-polarization transmission power increased from 17.2dB at 0.025mm to 26.6dB at 1mm, as shown in Fig.6. The transmission loss in passband for TE polarization incidence wave increased with the increasing of the thickness of the dielectric slabs.

The prototype of the frequency-selective polarizer was designed, fabricated and measured to validate the characteristics of the frequency-selective polarizer. The sample used was composed of 20 $\times$ 20 unit cells with total size of the printed circuit board(PCB) dimension of 14.4 cm$\times$14.4 cm. Fig.7 gives a photograph of the frequency-selective polarizer and a partial zoom-in of CSRR unit cells. The structure was modeled and simulated by the HFSS software which is based on finite element method(FEM). For simulation, the master/slaver boundaries and Floquet port were used in the modeling of the frequency-selective polarizer. The simulated results show that the pass-band was near the 10.275GHz with a transmission loss of 0.25dB for TE polarization incidence wave, while a significantly suppression with a 18dB transmission loss for TM polarization incidence wave at the CSRR resonant frequency.

III. RESULTS AND DISCUSSION

In the above sections, the performance of the novel CSRR-FSS polarizer at microwave regime was discussed according the simulation result. In this part, the experiment is carried out for validate the simulated predications. The measurement results were obtained using an HP E8364C vector network analyzer connecting two rectangle horn antennas in a transmission measurement setup.

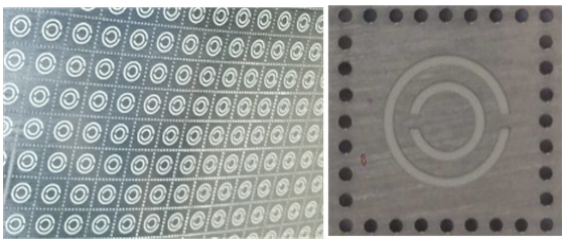

FIGURE 7. Photo of the prototype of the fabricated frequency-selective polarizer (a zoom-in CSRR unit cell).

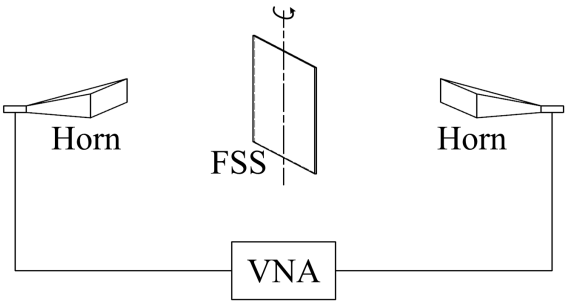

FIGURE 8. The measurement setup of the frequency-selective polarizer.

Fig.8 shows the schematic of the transmission measurement setup. The reasons for using the rectangle horn antenna is that the polarization of the radiation field at the far field could be accurately identified, because the excitation of the rectangle antenna is the TE_{10} mode for antenna feeding waveguide. Since the operating frequency range of rectangle horn antennas in experiment were restricted in X-band, so the testing was carried out in the frequency from 8GHz to 14GHz for getting more dependable measurement results.

A. CHARACTERISTICS OF THE POLARIZER AT NORMAL INCIDENCE

Fig.9 show the comparison of the simulated and measured results for TE/TM polarization excitation at the condition of normal incidence. As we can see from Fig.9, the measured results show that the minimum transmission loss for TE-polarization incidence wave is 0.75dB at 10.24GHz, but 19.05dB for the TM-polarization incidence wave at the same frequency(10.24GHz) with an extinction ratio of 18.3dB. These results suggest that the proposed CSRR-FSS is a TE-pass/TM-stop polarizer at the near frequency of the resonance of CSRRs particles(10.24GHz). The Fig.9 also indicated that the measurement results are in good agreement with the simulated predication. The errors of the frequency shift and transmission null point between simulated and measurement are mainly caused by the fabrication tolerances and the testing environment.

According to theory analysis in [18], when the incidence wave is polarized as TE mode for normal incidence and near the resonance of the CSRRs particles, a strong transmission peak would be expected at the frequency of resonance of the CSRRs particles, and an almost total reflection property would be seen for the orthogonal polarization (TM mode).

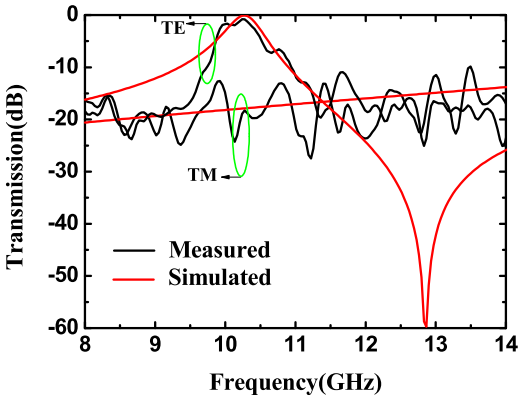

FIGURE 9. The measured and simulated transmission coefficient for the TE and TM polarization incidence wave.

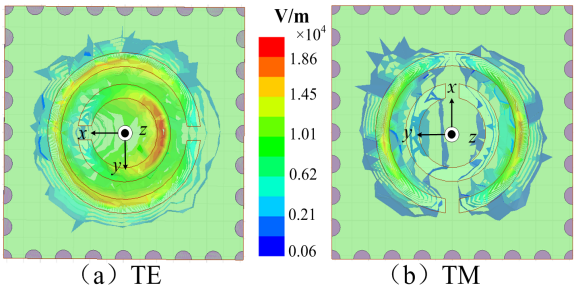

FIGURE 10. The electric field distribution in the dielectric box at the frequency(10.275GHz) of resonance of the CSRRs, magnitude depicted in colors. (a)TE mode incidence (b)TM mode incidence.

Therefore, the CSRR-FSSs act as a TE pass/TM stop polarizer, which have the ability to significantly suppress the transmission of the TM mode incidence wave, while well guiding the TE mode incidence wave at the near operation frequency.

In order to demonstrate the frequency-selective polarizer characteristics clearly, the electric field distributions in the dielectric box clamped between two stacked metallic layers is given at the operation frequency of the CSRR-FSS polarizer of (10.275GHz).

Fig.10 shows the electric field distribution in the dielectric box at the normal incidence wave for TE and TM polarization. According to [18], when the incidence wave is normal ($k_x = k_y = 0, k_z \neq 0$), the transmission waves have the same polarization as the incident wave. Let us consider the electric field distribution in Fig.10 (a), the transmission waves have the same polarization as the incidence waves which the electric field direction is perpendicular to y-z plane for TE mode incidence waves. The mode called gapped mode occurs when the CSRRs resonant at ω_0, which is caused by the superposition of an electric dipole mode and a magnetic dipole mode excited by the incidence waves. But in Fig.10 (b), because the transmission waves have the same polarization as the incidence waves which the electric field direction is perpendicular to x-z plane for TM mode incidence waves. As we can see from this picture, the electric distribution is mirror symmetry for the x-z plane, and the mirror symmetric field distribution would cause the mirror symmetric current distribution, which would make the radiation field perpen-

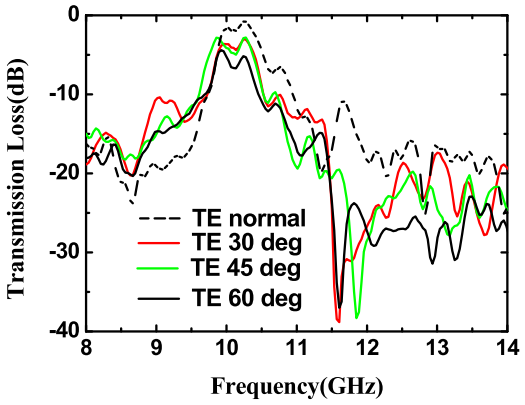

FIGURE 11. The measured transmission coefficient for the TE polarization incidence wave in different incidence angles (E perpendicular to y-z plane in Fig.10(a)).

dicular to *x*-*z* plane in the transmission area exactly canceled. So, the TM mode incidence wave cannot pass through the CSSR-FSSs screen.

B. CHARACTERISTICS OF THE POLARIZER AT OBLIQUE INCIDENCE

As we all know that for the FSS, the insusceptibility to changes of the incidence angles and stability of bandwidth is an important performance which may determine how useful of this kind of FSS screen in practical conditions.

Fig.11 gives the frequency response of the frequency-selective polarizer with TE-polarization and different angles incidence. From the figure we can find that the bandwidth is insensitivity to incidence angles from 0° to 45°, its stop-band beyond transmission null point is suppressed to below −20 dB. And the frequency resonance of the CSRRs particle shift to the lower end; the transmission loss in the pass-band increased evidently to 2-5dB with the angle increased from 30° to 60°.

This may be caused by the edge effect because of the CSRR-FSS screen with 20 × 20 CSRR elements and is not large enough. And the influence of the edge effect would be zoomed in when the incident angle was increased.

C. CHARACTERISTICS OF THE POLARIZER UNDER BENDING CONDITION

In the last decade, the flexible materials had been attracting wide attention in high frequency applications. The LCP substrate, as a promising bendable and flexible material, has also been showing its superiorities in applications of microwave and millimeter-wave circuits due to its features of excellent loss tangent (approximately 0.005 over the entire RF range up to 170 GHz), stable and desirable electrical characteristics for wide band, extremely low moisture absorption, and low thermal expansion coefficient [21], [34]. Fig.12 gives the schematic of the bending testing setup used to measure the flexibility of the frequency-selective polarizer and the calculation of the bending radius(*R*). The frequency-selective polarizer was fixed to the curved surface of a polystyrene foam in order to facilitate the measurement of the bending

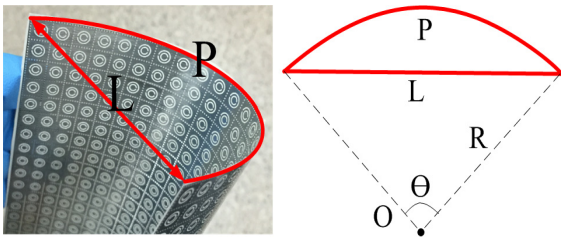

FIGURE 12. The schematic of the bending measurement setup and calculation of bending radius (R) for the proposed frequency-selective polarizer.

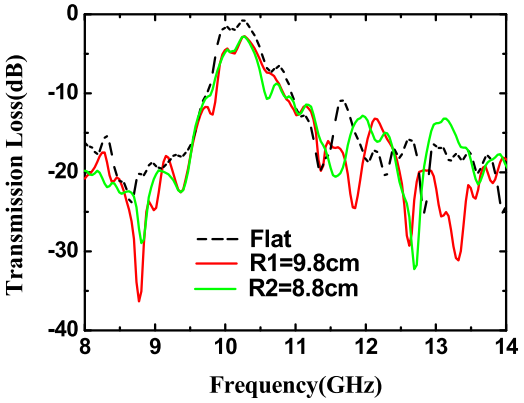

FIGURE 13. The measured transmission coefficient for the TE polarization incidence wave in different bending radius (E perpendicular to *y*-*z* plane in Fig.10(a)).

test, then the distance (*L*) between the opposite sides of the FSS array was extracted to calculate the bending radius (*R*) of the frequency-selective polarizer at bending condition situations. The reason for choosing foam as bending carrier to apply a tensile strain to the LCP substrate and achieve mechanical strain is that the dielectric constant of the foam is about 1.06 which is very close to the air's. The radius(*R*) satisfy the Equation (8) as followed:

$$\frac{L}{2R} = \sin\frac{P}{R} \tag{8}$$

Following the measurement flow shown in Fig.12, the bending experiments of the frequency-selective polarizer at the TE-polarization normal incidence and two different radius ($R_1 = 9.8$cm, $R_2 = 8.8$cm) conditions was carried out. Fig.13 gives the transmission loss of the frequency-selective polarizer before and after bending. The transmission loss under bending conditions increased to 2dB-3dB from 0.75dB at flat condition. However, the resonance frequency of CSRRs particles was not sensitive to the bending behavior of the LCP substrate. Which means that this CSRR structure of the frequency-selective polarizer is a promising candidate for the non-planar and conformal applications in the near future.

IV. CONCLUSION

In this paper, a novel method to designing and verifying a 10 GHz frequency-selective flexible polarizer was presented. The polarizer is composed of frequency selective surface (FSS) loaded complementary split ring resonator (CSRR) based on an ultra-thin liquid crystal polymers (LCP) substrate of 50μm thickness. The measured

results were good agree with the simulated results, showing that this frequency-selective polarizer have the characteristics of the minimum transmission loss for TE-polarization incidence wave is 0.75dB at 10.24GHz, but 19.05dB for the TM-polarization incidence wave with an extinction ratio of 18.3dB. The bending and oblique incidence tests show that this CSRR-FSS polarizers have acceptable deterioration to bending behavior and big angles incidence. The works in this paper may provide a useful guide for designing of the new structure polarizer covering the microwave to terahertz frequency range for the future non-planar and conformal applications.

REFERENCES

[1] W. Liu, M. Wang, and J. Yao, "Tunable microwave and sub-terahertz generation based on frequency quadrupling using a single polarization modulator," *J. Lightw. Technol.*, vol. 31, no. 10, pp. 1636–1644, May 15, 2013.

[2] T. Cai, G.-M. Wang, X.-F. Zhang, J.-G. Liang, Y.-Q. Zhuang, D. Liu, and H.-X. Xu, "Ultra-thin polarization beam splitter using 2-D transmissive phase gradient metasurface," *IEEE Trans. Antennas Propag.*, vol. 63, no. 12, pp. 5629–5636, Dec. 2015.

[3] D. W. Kim, M. H. Lee, Y. Kim, and K. H. Kim, "Planar-type polarization beam splitter based on a bridged silicon waveguide coupler," *Opt. Exp.*, vol. 23, no. 2, pp. 998–1004, 2015, doi: 10.1364/OE.23.000998.

[4] M. N. Abbas, C.-W. Cheng, Y.-C. Chang, and M. H. Shih, "An omnidirectional mid-infrared tunable plasmonic polarization filter," *Nanotechnology*, vol. 23, no. 44, Nov. 2012, Art. no. 444007.

[5] Y. Cui, Q. Wu, E. Schonbrun, M. Tinker, J.-B. Lee, and W. Park, "Silicon-based 2-D slab photonic crystal TM polarizer at telecommunication wavelength," *IEEE Photon. Technol. Lett.*, vol. 20, no. 8, pp. 641–643, Apr. 2008.

[6] Q. Bao, H. Zhang, B. Wang, Z. Ni, C. H. Y. X. Lim, Y. Wang, D. Y. Tang, and K. P. Loh, "Broadband graphene polarizer," *Nature Photon.*, vol. 5, no. 7, pp. 411–415, May 2011, doi: 10.1038/NPHOTON.2011.102.

[7] R. Mittra, C. H. Chan, and T. Cwik, "Techniques for analyzing frequency selective surfaces-a review," *Proc. IEEE*, vol. 76, no. 12, pp. 1593–1615, Dec. 1988.

[8] Q. Chen and Y. Fu, "A planar stealthy antenna radome using absorptive frequency selective surface," *Microw. Opt. Technol. Lett.*, vol. 56, no. 8, pp. 1788–1792, Aug. 2014.

[9] Y. C. Chang, "Low radar cross section radome," U.S. Patent 6 639 567 B2, Oct. 28, 2003.

[10] J. B. Pendry, A. J. Holden, D. J. Robbins, and W. J. Stewart, "Magnetism from conductors and enhanced nonlinear phenomena," *IEEE Trans. Microw. Theory Techn.*, vol. 47, no. 11, pp. 2075–2084, Nov. 1999.

[11] N. A. Estep, A. N. Askarpour, and A. Alù, "Experimental demonstration of negative-index propagation in a rectangular waveguide loaded with complementary split-ring resonators," *IEEE Antennas Wireless Propag. Lett.*, vol. 14, pp. 119–122, 2015.

[12] F. Martin, J. Bonache, F. Falcone, M. Sorolla, and R. Marques, "Split ring resonator-based left-handed coplanar waveguide," *Appl. Phys. Lett.*, vol. 83, no. 22, pp. 4652–4654, Dec. 2003.

[13] J. D. Baena, L. Jelinek, J. J. Mock, J. Gollub, R. Marques, and D. R. Smith, "Isotropic frequency selective surfaces made of cubic resonators," *Appl. Phys. Lett.*, vol. 4, no. 7, pp. 1228–1236, Jul. 2014.

[14] S. Ya and A. E. Vandenbosch, "Compact circular polarizer based on chiral twisted double split-ring resonator," *Appl. Phys. Lett.*, vol. 102, Feb. 2013, Art. no. 103503, doi: 10.1063/1.4794940.

[15] R. M. S. Cruz, P. H. da F. Silva, and A. G. D. Assuncao, "Neuromodeling stop band properties of Koch Island patch elements for FSS filter design," *Microw. Opt. Technol. Lett.*, vol. 51, no. 12, pp. 3014–3019, Dec. 2009, doi: 10.1002/mop.24795.

[16] F. Falcone, T. Lopetegi, M. A. G. Laso, J. D. Baena, J. Bonache, M. Beruete, R. Marqués, F. Martín, and M. Sorolla, "Babinet principle applied to the design of metasurfaces and metamaterials," *Phys. Rev. Lett.*, vol. 93, no. 19, pp. 7401–7405, Nov. 2004, doi: 10.1103/physrevlett.93.197401.

[17] Z. Y. Wei, Y. Gao, Y. C. Fan, and H. Q. Li, "Broadband polarization transformation via enhanced asymmetric transmission through arrays of twisted complementary split-ring resonators," *Appl. Phys. Lett.*, vol. 99, Sep. 2014, Art. no. 221907, doi: 10.1063/1.3664774.

[18] R. Marques, J. D.Baena, M. Beruete, F. Falcone, T. Lopetegi, M. Sorolla, F. Martin, and J. Garcia, "Ab initio analysis of frequency selective surfaces based on conventional and complementary split ring resonators," *J. Opt. A, Pure Appl. Opt.*, vol. 7, pp. S38–S43, Jan. 2005, doi: 10.1088/1464-4258/7/2/005.

[19] G. B. Philippe and J. F. Martin, "Electromagnetic resonances in individual and coupled split-ring resonators," *J. Appl. Phys.*, vol. 92, p. 2929, Dec. 2015.

[20] N. Katsarakis, T. Koschny, and M. Kafesaki, "Electric coupling to the magnetic resonance of split ring resonances," *Appl. Phys. Lett.*, vol. 84, no. 15, pp. 2943–2945, Apr. 2004.

[21] C. Dagdeviren, Y. W. Su, P. Joe, R. Yona, Y. H. Liu, Y. S. Kim, Y. A. Huang, A. R. Damadoran, J. Xia, L. W. Martin, Y. G. Huang, and J. A. Rogers, "Conformable amplified lead zirconate titanate sensors with enhanced piezoelectric response for cutaneous pressure monitoring," *Nature Commun.*, vol. 5, Aug. 2014, Art. no. 4496, doi: 10.1038/ncomms5496.

[22] S. Yang, P. Liu, M. D. Yang, Q. G. Wang, J. M. Song, and L. Dong, "From flexible and stretchable meta-atom to metamaterial: A wearable microwave meta-skin with tunable frequency selective and cloaking effects," *Sci. Rep.*, no. 6, Feb. 2016, Art. no. 4496, doi: 10.1038/srep21921.

[23] A. C. M. Division and R. Corporation. (2014). *ULTRALAM 3000 Liquid Crystalline Polymer Circuit Material*. [Online]. Available: http://www.rogerscorp.com

[24] H. L. Kao, C. S. Yeh, X. Y. Zhang, C. L. Cho, X. Dai, B. H. Wei, L. C. Chang, and H. C. Chiu, "Inkjet printed series-fed two-dipole antenna comprising a balun filter on liquid crystal polymer substrate," *IEEE Trans. Compon., Packag., Manuf. Technol.*, vol. 4, no. 7, pp. 1228–1236, Jul. 2014.

[25] Y. Lan, Y. H. Xu, C. S. Wang, Z. Wen, Y. J. Qiu, T. D. Mei, Y. Q. Wu, and R. M. Xu, "X-band flexible band-pass filter based on ultra-thin liquid crystal polymer substrate," *Electron. Lett.*, vol. 51, no. 4, pp. 345–347, Feb. 2015.

[26] Y. H. Jung, "A compact parylene-coated WLAN flexible antenna for implantable electronics," *IEEE Antennas Wireless Propag. Lett.*, vol. 15, pp. 1382–1385, 2016.

[27] S. M. A. Momeni Hasan Abadi and N. Behdad, "Wideband linear-to-circular polarization converters based on miniaturized-element frequency selective surfaces," *IEEE Trans. Antennas Propag.*, vol. 64, no. 2, pp. 525–534, Feb. 2016.

[28] G. Q. Luo, W. Hong, Z.-C. Hao, B. Liu, W. D. Li, J. X. Chen, H. X. Zhou, and K. Wu, "Theory and experiment of novel frequency selective surface based on substrate integrated waveguide technology," *IEEE Trans. Antennas Propag.*, vol. 53, no. 12, pp. 4035–4043, Dec. 2005.

[29] Y. L. Zhang, W. Hong, K. Wu, J. X. Chen, and H. J. Tang, "Novel substrate integrated waveguide cavity filter with defected ground structure," *IEEE Trans. Microw. Theory Techn.*, vol. 53, no. 4, pp. 2075–2084, Apr. 2005.

[30] D. Deslandes and K. Wu, "Single-substrate integration technique of planar circuits and waveguide filters," *IEEE Trans. Microw. Theory Techn.*, vol. 51, no. 2, pp. 593–596, Feb. 2003.

[31] S. A. Winkler, W. Hong, M. Bozzi, and K. Wu, "Polarization rotating frequency selective surface based on substrate integrated waveguide technology," *IEEE Trans. Antennas Propag.*, vol. 58, no. 4, pp. 1202–1213, Apr. 2010.

[32] X.-C. Zhu, W. Hong, K. Wu, H.-J. Tang, Z.-C. Hao, J.-X. Chen, H.-X. Zhou, and H. Zhou, "Design of a bandwidth-enhanced polarization rotating frequency selective surface," *IEEE Trans. Antennas Propag.*, vol. 62, no. 2, pp. 940–944, Feb. 2014.

[33] R. Marques, F. Mesa, J. Martel, and F. Medina, "Comparative analysis of edge− and broadside-coupled split ring resonators for metamaterial design–theory and experiments," *IEEE Trans. Antennas Propag.*, vol. 51, no. 10, pp. 2572–2581, Oct. 2003.

[34] D. C. Thompson, O. Tantot, H. Jallageas, G. E. Ponchak, M. M. Tentzeris, and J. Papapolymerou, "Characterization of liquid crystal polymer (LCP) material and transmission lines on LCP substrates from 30 to 110 GHz," *IEEE Trans. Microw. Theory Techn.*, vol. 52, no. 4, pp. 1343–1352, Apr. 2004.